Original Article
Endothelial remodeling in osteosarcomas: insights from patient samples and in vitro studies

Mélanie Legrand[1,2], Sarah Renault[1], Gonzague de Pinieux[1,2], Clara Bourreau[1], Régis Brion[1,4], Louis-Romée Le Nail[5], Stéphanie Blandin[6], Philippe Hulin[6], Franck Verrecchia[1,4], Françoise Rédini[1,4], Valérie Trichet[1,3*], Isabelle Corre[1,4*]

[1]Nantes Université, Inserm UMR 1238, F-44000 Nantes, France; [2]Université de Tours, CHRU, Service d'Anatomie Pathologique, F-37044 Tours, France; [3]Nantes Université, INSERM U1229, RMeS, F-44000 Nantes, France; [4]Nantes Université, Inserm UMR 1307, CNRS UMR 6075, Université d'Angers, CRCl2NA, F-44000 Nantes, France; [5]Université de Tours, CHRU, Service de Chirurgie Orthopédique et Traumatologie, CNRS ERL 7001 LNOx EA 7501 GICC, F-37044 Tours, France; [6]Nantes Université, CHU Nantes, CNRS, Inserm, BioCore, US16, SFR Bonamy, F-44000 Nantes, France. *Co-last authors.

Abstract: Osteosarcomas (OS) are the most frequent malignant primary bone sarcomas with an overall poor prognostic for high-risk patients. The current therapeutic management combining chemotherapy and surgery remains partially inefficient. OS are very heterogeneous tumors, evolving in a complex and specific highly vascularized microenvironment. Upon microenvironmental signals, remodeling of tumor vessels may occur through angiogenic processes but also through endothelial differentiation process namely the endothelial-to-mesenchymal transition (EndoMT). In a patient cohort of ten high-grade OS samples (at diagnosis, after surgery, and/or metastasis), we detected by a multiplexing immunohistochemistry approach the presence of endothelial cells co-expressing endothelial CD31/EMCN and mesenchymal ASMA/FSP1 markers. In order to partially mimic an OS microenvironment in vitro, we exposed human umbilical vein endothelial cells (HUVECs) to secreted factors of OS tumor or stromal cells. In this cellular model, we established that the secretome from stromal cells did not induce EndoMT in primary ECs. Nevertheless, soluble factors from the OS cell line KHOS were able to induce in ECs some of the EndoMT hallmarks such as induction of mesenchymal markers associated to increased migration, but without inhibition of tubulogenesis. In conclusion, this study identified the presence of endothelial-mesenchymal cells in the tumor microenvironment of OS patients and give cues for further investigation of the regulation and consequences of this remodeling in the biology of OS.

Keywords: Osteosarcoma, endothelial cells, remodeling, endothelial-to-mesenchymal transition, multiplexing immunochemistry

Introduction

Osteosarcomas (OS) are the most common primary malignant bone tumor, mainly affecting children, adolescents and young adults [1]. These tumors develop mainly in the long bones (tibia, humerus) close to the bone metaphysis, and less frequently in the skull, jaw and pelvis. OS are characterized by the presence of transformed osteoblastic cells producing osteoid matrix, leading to inappropriate and pathological bone remodeling. Cellular origin of OS is still not fully elucidated, but recent evidence supports the involvement of a skeletal stem cell [2-4]. Despite the introduction of chemotherapy before and after surgery resection of the tumor, the 5-year survival, that reached 78% for children and young adults with localized disease, has not been improved further for the last four decades and did not improve at all for metastatic patients or patients not responding to chemotherapy, remaining at 20% [1, 5, 6]. Therefore, improving therapy in OS remains a constant and major goal to reach. OS are very heterogeneous tumors both at the intra- and inter-tumor level and common genomic initiating biological processes driving the osteosarcomagenesis are not yet fully identified. Several

hereditary syndromes (*i.e.,* Li-Fraumeni, familial retinoblastoma cancers...) have also been associated with a predisposition to develop OS but these sarcomas appear as sporadic events in their vast majority [7]. Overall, poorly defined oncogenic events associated with high heterogeneity of OS tumor cells block the development of oncogene-targeted therapies.

OS tumor cells grow in the bone microenvironment, a very complex and dynamic environment composed of bone cells (osteoclasts, osteoblasts, osteocytes), stromal cells (mesenchymal stem cells (MSCs), fibroblasts), vascular cells (endothelial cells (ECs) and pericytes), immune cells (macrophages, lymphocytes) surrounded by a mineralized extracellular matrix (ECM). In physiological conditions, a coordinated and fine-tuned orchestrated activity between bone, vascular and stromal cells assure bone homeostasis, through intense paracrine and cellular communications. According to Paget's theory [8], tumor cells find there a fertile soil to seed and to develop and manage to highjack bone physiological pathways to their advantage in order to develop and survive. The endothelial compartment is a major actor in this tumor supportive microenvironment, mainly through the process of angiogenesis that provides new vessel required by the tumor for oxygen and nutriments [9]. OS are highly angiogenic vascularized tumors evolving in a hypoxic and acidic microenvironment and neo-vascularization markers such as VEGF (Vascular endothelial growth factor) and its receptor VEGF-R2 are associated with poor prognosis in patients [10, 11]. But beside their role in angiogenesis, ECs are also now described for their capacity to transdifferentiate into mesenchymal cells through the process of endothelial-to-mesenchymal transition (EndoMT). Initially described in normal heart development [12], EndoMT is now implicated in several fibrotic diseases [13]. Recent studies have characterized the EndoMT process in the tumor context mainly in lung cancer [14], colorectal cancer [15] and melanoma [16]. In the context of cancer, EndoMT has been associated with several important consequences: disruption of the endothelial barrier, facilitating dissemination of cancer cells [17] and generation of a source of carcinoma-associated fibroblasts [16]. Therefore, remodeling of the endothelial compartment has to be considered as an important issue in the supportive dialogue between ECs from the vascular micro-environment and cancer cells. Nevertheless, EndoMT transition process has never been yet investigated in primary bone tumors.

EndoMT has been documented on patient samples in several types of cancer [15, 16, 18, 19] and more recently in cervical squamous cell carcinoma [20] by immuno-detection of endothelial cells co-expressing specific endothelial marker CD31/PECAM (Platelet Endothelial Cell Adhesion Molecule-1), and mesenchymal markers such as ASMA (alpha smooth muscle actin) or FSP1 (fibroblast-specific protein 1, also named S100A4). Based on these approaches, we aimed at identifying such endothelial cells co-expressing endothelial markers CD31 together with mesenchymal markers (ASMA and/or FSP-1) in a collection of samples from high-grade OS patients at different stages (diagnosis, metastasis and resection post-treatment) and we include an additional endothelial marker Endomucin (EMCN), described as specific for endosteal and metaphysic bone vasculature [21]. In order to extend our understanding of endothelial remodeling in OS, we completed our work with an *in vitro* approach and explored the effects of the secretome of two human OS cell lines (KHOS and U2OS) and of mesenchymal stromal cells (MSCs) from OS patients on the remodeling of endothelial cells.

Materials and methods

Patient samples

The study was planned of a monocentric retrospective cohort constituted between 2015 and 2019 (Tours University Hospital, France) comprising 10 patients with osteosarcoma. Samples were obtained from patients during orthopedic surgery procedures in Tours University Hospital and written consent was obtained from informed patients in accordance with French law (Art. L. 1245-2 of the French public health code, Law No. 2004-800 of 6 August 2004, Official Journal of 7 August 2004). Tissue samples were formalin-fixed, decalcified for some samples and paraffin-embedded. The slides have been proof-read by two pathologists from an expert center in bone sarcomas. Clinical informations (gender, age at diagnosis, tumor location, histological subtype namely osteoblastic, fibroblastic, chondroblastic, telangectatic) were available in all cases. Their characteristics are summarized in **Table 1**.

Table 1. Clinical characteristics of ten patients diagnosed with high-grade osteosarcoma (OS)

Patient	A	B	C	D	E	F	G	H	I	J
Year of diagnosis	2015	2016	2016	2017	2017	2018	2018	2019	2019	2019
Age	12	17	14	11	16	18	8	19	47	14
Gender	M	F	M	F	F	F	F	M	M	M
Tumor site	Distal femur	Humerus	Proximal tibia	Distal femur	Distal femur	Proximal tibia	Humerus	Distal femur	Leg muscle	Distal femur
Histological subtype	OB, F	OB, CH	OB	OB, CH	F, T	OB	OB	F	OB, CH	OB, CH
Response to NAPC	PR	PR	PR	GR	GR	GR	GR	PR	PR	GR
% Residual tumor cells	30	50	25	1	0	0	0	35	66	3
Metastasis at diagnosis	No	No	Yes	No	Yes	No	No	Yes	No	No
Local recurrence	No	No	No	No	No	No	No	No	No	No
Metastasis progression	Yes (lung)	Yes (lung)	No	Yes (lung)	Yes (brain)	No	No	Yes (lung; spinal)	Yes (lung; kidney; bone; muscle)	No
Outcomes	DOD	DOD	NED	AWD	DOD	NED	NED	NED	AWD	NED

Alphabetic letter identification was chosen for patients. Year of diagnosis, age, male (M) and female (F) gender at diagnosis were indicated. Histological subtypes were osteoblastic (OB), chondroblastic (CH), fibroblastic (F), telangiectatic (T) or a combination of those different subtypes. Response to neo-adjuvant polychemotherapy (NAPC) was indicated as good (GR) or poor (PR) depending on the % of residual tumor cells counted on histological analysis of tumor resection pieces, respectively, less or greater than 10%. Presence and location of metastasis at the time of diagnosis were identified. Patient outcomes were noted either dead of disease (DOD), or alive with disease (AWD), or alive with no evidence of disease (NED).

Multiplex staining with OPAL™ multiplex immu-nohistochemistry assay

Tissue preparation for staining: In brief, formalin-fixed paraffin embedded tissue sections were heated at 60°C for 1 hour, deparaffinized with series of xylenes, and rehydrated by serial passage through grade concentrations of ethanol. Tumor samples were decalcified according to the recommendations published by the French bone pathology group, *i.e.* the use of a weak acid, formic acid, over a reduced number of short cycles, allowing optimal antigen detection [22]. Hematoxylin-eosin saffron staining was performed on each sample to select sections with cell viability above 5% for immuno-histology analysis. For some of them, poor tissue integrity was revealed, mainly due to cell death induced by chemotherapeutic treatments and/or due to the storage of samples.

Singleplex and multiplex immunofluorescence: Immunohistochemistry analysis was performed by using the following antibodies: rabbit anti-human CD31 (endothelial cells positive, dilution 1:50, Abcam, Cambridge UK, ab28364), rabbit anti-human EMCN (endothelial cells positive, dilution 1:250, Invitrogen, PA5-21395), mouse anti-human ASMA (mesenchymal/smooth muscle cells positive, dilution 1:1600, R&D Systems, MAB1420), rabbit anti-human FSP1 (mesenchymal/fibroblast cells positive, dilution 1:250, Abcam, UK, ab124805), diluted in blocking solution for 1 hour at room temperature.

Multiplexed immunofluorescence staining was performed using Akoya Opal reagent on the immunostaining automaton Impath 36 (A. Menarini, Diagnostics). Each primary antibody was paired to a select Opal Fluorophore and single stained. Opal fluor-marker pairings were based on known brightness rankings, with more abundant markers paired with less bright fluorophores and inversely. The Opal fluorophores were used at 1/200 dilution, in the 1X Tyramide Plus Automation Amplification Diluent (Akoya, ref. FP1609). As such, a fluorescent singleplex was performed for each biomarker and compared to the appropriate chromogenic singleplex to assess staining performance. During multiplex optimization, Opal-antibody pairings and denaturing parameters for each biomarker were assessed and adjusted. Using

the Opal method (Akoya) after deparaffinization, four primary antibodies were sequentially applied to a single slide. Antigen retrieval was performed in citrate buffer (pH 6.0, Dako, K8005) using water bath treatment followed by cooling at room temperature. Tissue sections were blocked with blocking agent (H_2O_2) and incubated for 1 hour with primary antibody against ASMA (1:1600) followed by detection using HRP poly-E and HRP-2-step (Impath, ref 46538), used as secondary antibody. Visualization of ASMA was accomplished using Opal 520 Fluorophore (1:200), after which, antigen retrieval TR1 pH 9.0 solution (Impath, ref 44999) was deposited on the slide and heated. The slides were then incubated with EMCN antibody (1:250) for 1 hour, followed by detection using the Polymer HRP. EMCN staining was visualized using Opal 540 Fluorophore (1:200). Slides were placed in EDTA-buffer (pH 9.0) and subjected to water bath treatment and then incubated with primary antibodies for FSP1 (1:250) for 1 hour, followed by detection using the Polymer HRP. FSP1 staining was visualized using Opal 620 Fluorophore (1:200), after which, antigen retrieval solution TR1 pH 9.0 solution (Impath, ref 44999) was deposited on the slide and heated. Slides were then incubated with CD31 (1:50) for 1 hour, followed by detection using the Polymer HRP and visualization using Opal 690 Fluorophore (1:200). Then, nuclei were labeled with 4',6-diamidino-2-phenylindole solution DAPI (Molecular Probes, ref D1306), and the sections were cover-slipped using mounting medium (Vectashield® Vibrance™ Antifade Mounting Medium, Vector Laboratories, ref H-1700). Immunofluorescence staining lacking the relevant primary antibody was used as negative control.

Image acquisition: Confocal spectral laser microscopy was performed using Nikon A1R-Si microscope with NIS software V5.21 (Nikon France SAS, Champigny-sur-Marne). First, spectral signature of each Opal used (520/540/620/690) was independently recorded on the initial tissue by spectral microscopy mode using 32 photomultiplier detectors with a 2.5 nm step. Then, each sample was scanned sequentially with four lasers (405/488/561/647 nm) and each acquisition was unmixed with NIS to reveal the spectrum of each OPAL initially determined. Three to 16 acquisitions were carried out by sample, depending on its quality. All

the images were analyzed by Image J software (NIH, Bethesda, MD, USA).

Cell culture and treatments

Pooled human umbilical vein endothelial cells HUVEC (Lonza, Belgium) were grown in Endothelial Cell Growth Medium EGM2, composed of Endothelial Cell Basal Medium EBM2 supplemented with Single Quots and 2% fetal bovine serum (FBS) as described by the manufacturer at 37°C in a 5% CO_2 humidified air incubator. OS cell lines HOS (CRL-1544) and U2OS (HTB-96) were purchased from ATCC (LGC Standards, France). Cells were cultured in DMEM (Dulbecco's Modified Eagle's Medium, Lonza, Switzerland) supplemented with 10% FBS (HayclonePerbio, France). HUVECs were treated with 10 ng/ml recombinant human of TGF-β2 and IL-1β (Miltenyi Biotec, Germany) for 6 days. Mesenchymal stromal cells (MSCs) and osteosarcoma derived cells (OSDCs) were obtained as previously described [23]. Briefly, MSCs were extracted from normal bone marrow, while OSDCs were derived from OS biopsy of patient I. MSCs and OSDCs were cultured in Minimum Essential Medium alpha (α-MEM) with nucleosides and 1 g/L D-Glucose (Gibco®, Life technologies, France), supplemented with 1% antibiotics (Penicillin 100 U/ml and Streptomycin 100 mg/l; Invitrogen, France), 10% FBS and 1 ng/mL basic-Fibroblast Growth Factor (bFGF), at 37°C in a humidified atmosphere (5% CO_2/95% air). MSCs and OSDCs were seeded at 2500 cells per cm^2 between passage 1 to 8. Cells were characterized by flow cytometry and for their potential for osteoblast differentiation.

Preparation of conditioned media

OS cell lines were cultured up to 80% confluency in DMEM, 10% FBS at 37°C in a 5% CO_2 humidified air incubator. Medium was then replaced by EBM2 for 24 hours. Supernatant was harvested, centrifuged at 2500 rpm for 10 minutes. Conditioned media from MSCs and OSDCs were obtained from sub-confluent cells cultured for 48 hours in EBM2, 2% FBS and were spined. Collected EBM2-conditioned media were then supplemented with Single Quots to reconstitute an EGM2-supernatant and were incubated on HUVECs for 6 days. The control of conditioned media (CM-control) was composed of EBM2 medium incubated 48 hours at 37°C,

5% CO_2, then supplemented up to EGM2 composition.

Migration assay

After 6 days of exposure to TGF-β2/IL-1β or to conditioned media (CM) from OS cell lines, MSCs or OSDCs, HUVECs were harvested and 50000 cells were seeded in free-serum medium on a Transwell® insert with 8 μm pores size into a Boyden chamber with the lower chamber filled with 2% FBS. Cells were incubated for 8 hours at 37°C. Then, cells at the upper face were removed and cells at the lower face of the membrane were fixed with 1% glutaraldehyde and stained with crystal violet. Migrated cells were counted using Image J software, in 14 fields of view (FOV) per insert and then represented as mean of cells/FOV.

Tubulogenesis assay

After 6 days of exposure to TGF-β2/IL-1β or CM, HUVECs were harvested and 7500 cells were plated on growth factor-reduced Matrigel® in μ-slide angiogenesis Ibidi-Treat in EGM2 medium (Clinisciences, France). Cells were incubated for 6 hours at 37°C and formation of tubes was observed by microscopy at 10× magnification. Branching points were counted using Image J software.

Detection of TGF-β2 in OS cell lines conditioned medium

Supernatant of 48 hours-cultured KHOS and U2OS cells were assessed by the Bio-Plex® system (Luminex, Bio-Rad, France). Concentration of TGF-β1 and -β2 were measured in CM using Milliplex MAP kits (Merck Millipore, France). The procedure was performed according to the manufacturer's protocols. Each sample concentration was calculated using a 5-parameter logistic fit curve generated from the standards and expressed in pg/mL.

RT-qPCR analysis of endothelial and mesenchymal genes

Total RNA was extracted from cells using Nucleospin RNA Plus Kit (Macherey-Nagel, France) according to manufacturer's instructions. First-strand cDNA was synthesized from 1 μg of total RNA using Maxima H Minus First Strand cDNA Synthesis Kit (Fisher Scientific,

France) with Primer Oligo (dT). Quantitative Real Time PCR was performed using 20 ng of cDNA using the SYBR select master mix (Life Technologies; Thermofisher, France) and CFX96 Real Time PCR detection system (BioRad, France). Primer sequences used for RT-qPCR are listed in Supplementary Table 1. The relative mRNA quantification was calculated using $2^{-\Delta\Delta Ct}$ and $2^{-\Delta Ct}$ methods and normalized by two housekeeping genes *HPRT* (hypoxanthine-guanine phosphoribosyl transferase) and *B2M* (beta-2-microglobulin). All the experiments were repeated at least 3 times in triplicate.

Statistics

Data are representative of at least three independent experiments. Statistical analyses were performed with GraphPad Prism8 (GraphPad Software, CA) using two-way ANOVA or Mann-Whitney test. A *p*-value under or equal to 0.05 was considered statistically significant.

Results

Clinical characteristics of a cohort of ten patients with high-grade OS

Tissue samples included in this prospective histological study were from patients with high-grade OS at first diagnosis at Tours University Hospital (no inclusion of patients with low-grade) and have been collected between 2015 and 2019. This new cohort of ten patients included an equal gender ratio and a median of 15 years old (**Table 1**). All patients except the oldest patient I (47 years old) presented a tumor location in long bones (femur, humerus, or tibia) concordant with the prevalent location of high-grade OS. Patient I's disease was located in leg muscle; however, its histological subtype was osteoblastic and chondroblastic as predominantly observed with other patients. A rare telangiectatic subtype was observed with patient E. Neo-adjuvant poly-chemotherapy (NAPC) resulted in poor response and high tumor cell survival for 50% of patients, while surgical resection prevented local recurrence for 100% of patients. The presence of metastasis at diagnosis classified three patients (patients C, E and H) as having the most severe grade of disease; fortunately, no evidence of disease was observed for two of them until 2023 following treatment. In contrast, four patients (patients A, B, D and I) with no metas-

tases at diagnosis, then presenting a less severe grade of OS, had either died of the disease or were alive with disease at the last point of this study after treatment. Regarding this small cohort of patients with a relatively young disease, neither the response to NAPC nor the presence of metastasis at diagnosis can be related to recent outcomes. Patient C was still alive with no evidence of disease (NED) despite a poor response to NAPC and with metastasis at diagnosis. In contrast, patient E diagnosed few months later than patient C, also with metastasis, had a good response to NAPC but died of the disease (DOD). No gender differences were observed in response to NAPC, metastases at diagnosis or progression, or outcomes in this small cohort made of five women and five men.

Endothelial cells expressed mesenchymal markers on human samples of high-grade OS

From the cohort described above, Hematoxylin Eosin Saffron (HES) staining of tissue sections was performed on all samples (biopsies, surgery resection pieces, and metastasis). Then, we used an Opal™ multiplexing approach using specific primary antibodies previously used for the detection of two endothelial markers CD31 and EMCN, and of two mesenchymal markers, ASMA and FSP1. These markers were used in combination with DAPI nucleus staining. As validation of these antibodies was previously performed on non-tumor area of the patient I lung sample (data not shown), the initial multiplexing approach was performed on this lung sample within the tumor metastasis tissue (**Figure 1**). This sample presented numerous vessels and high cellular integrity, as patient I had not been treated with chemotherapy before resection of lung metastases (**Figure 1A**). ECs have been identified as cells lining the lumen of a blood vessel with a DAPI-stained nucleus associated with CD31 staining (**Figure 1B**, pink arrows). Among these CD31-positive cells, some but not all were co-expressing EMCN and they were all considered as ECs and termed CD31+EMCN+/- (**Table 2**). Among these ECs, confocal imaging and spectral confocal acquisition allowed the detection of several cells co-expressing the mesenchymal marker ASMA (**Figure 1B**, white arrows). Thus, endothelial cells CD31+EMCN+/- co-expressing ASMA were denominated endothelial-mesenchymal cells (EndoMCs). ASMA-
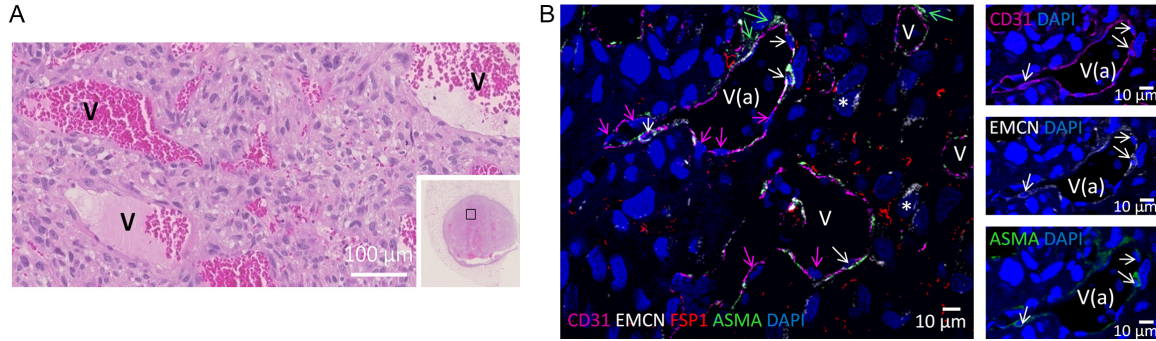
Figure 1. Representative microphotographies of multiplex immunofluorescent staining of vessels validated on chemotherapy-naive and not decalcified lung samples (patient I). A. Image of lung sample section after hematoxylin-eosin saffron staining. Lumen of vessels was indicated (V) Scale Bar: 100 μm. B. Images of multiplexed immunofluorescent histochemistry on vessels termed V and V(a). Each marker was related to the detection of a specific fluorochrome and was presented with the color code indicated in merged pictures. Single fluorescent images were shown for vessel V(a). Pink arrows showed nuclei (labeled with DAPI) of endothelial cells (ECs) expressing CD31, associated or not with EMCN expression, whereas white arrows showed ECs expressing CD31, associated or not with EMCN expression, and mesenchymal marker ASMA. Green arrows showed ASMA-positive cells that were distinguished from ECs and may correspond to smooth muscle cells. Asterisks indicated some large nuclei of tumor cells expressing EMCN. Scale Bars: 10 μm.

Table 2. Endothelial cells (ECs) and endothelial-mesenchymal cells (EndoMCs) detected in human osteosarcoma (OS) samples

PATIENT	BIOPSY									RESECTION				METASTASIS
	B	C	D	E	F	G	I	J	Mean (SD)	A	B	H	Mean (SD)	I
Nber of Vessels	1	6	5	17	14	3	2	9	9.3 (8.9)	4	4	15	7.7 (6.4)	26
Nber of ECs (CD31$^+$EMCN$^{+/-}$)	3	7	15	12	19	11	10	58	20.9 (28.3)	26	13	6	15 (10.1)	47
Nber of EndoMCs (CD31$^+$EMCN$^{+/-}$ and ASMA$^+$)	0	3	0	0	0	0	1	10	1.75 (3.5)	13	2	3	6 (6.1)	15
% EndoMCs (NberEndoMCs/ECs)	0	42	0	0	0	0	10	17	8 (14.9)	50	15	50	38.5 (20)	32

Histological section of osteosarcoma biopsies, resection piece and metastases were used in a multiplexed immunofluorescent histochemistry assay and observed by confocal microscope. Vessels were counted on each histological section. Endothelial cells (ECs) were identified as cell positioned in the inner layer of a blood vessel, with nuclei labeled with DAPI and with a specific endothelial fluorescent signal corresponding to the detection of CD31 (also known as platelet endothelial cell adhesion molecule, PECAM-1). Among these ECs, a few cells presented a supplementary specific mesenchymal fluorescent signal corresponding to the detection of either Fibroblast-specific protein 1 (FSP1, also named S100A4) or alpha smooth muscle actin (ASMA); these double-stained cells were identified as endothelial-mesenchymal cells (EndoMCs). Numbers of ECs and EndoMCs were reported for each histological section; mean with standard deviation of ECs or EndoMCs were presented for OS biopsy and resection samples. The percentage of EndoMCs among the total number of ECs was calculated.

expressing ECs were distinct from ASMA-positive mural cells (smooth muscle cells or pericytes) that were separated from ECs by an unstained space (**Figure 1B**, green arrows). FSP1 was not found expressed in ECs of OS samples, but was detected in tumor connective tissue. Surprisingly, EMCN expression was not restricted to ECs but was associated with some tumor cells (**Figure 1B**).

With these encouraging results on lung metastasis sample, endothelial and mesenchymal markers were sought in biopsies of the cohort described above. Biopsy samples (n=8) were analyzed by multiplexing approach. As shown in **Figure 2** which presents images of osteoblastic and chondroblastic OS histological sub-

type (**Figure 2A**, patients I and J), the presence of CD31-positive cells expressing mesenchymal ASMA was detected (**Figure 2B**, white arrows). As observed in lung metastasis, EMCN expression was not restricted to ECs but was also associated with large nuclei of some tumor cells, and eventually associated with ASMA staining. As EMCN-positive tumor cells bordering vessels and evoking vascular mimicry were detected in few samples (**Figure 2** with patient I; Supplementary Figure 1 with patient B), we considered as ECs, only the cells expressing at least CD31 (with or without EMCN) and presenting a nucleus bordering the lumen of a vessel. EndoMCs (CD31$^+$EMCN$^{+/-}$ASMA$^+$) were quantified and results presented in **Table 2**. Three patient's biopsies out of 8 had detect-
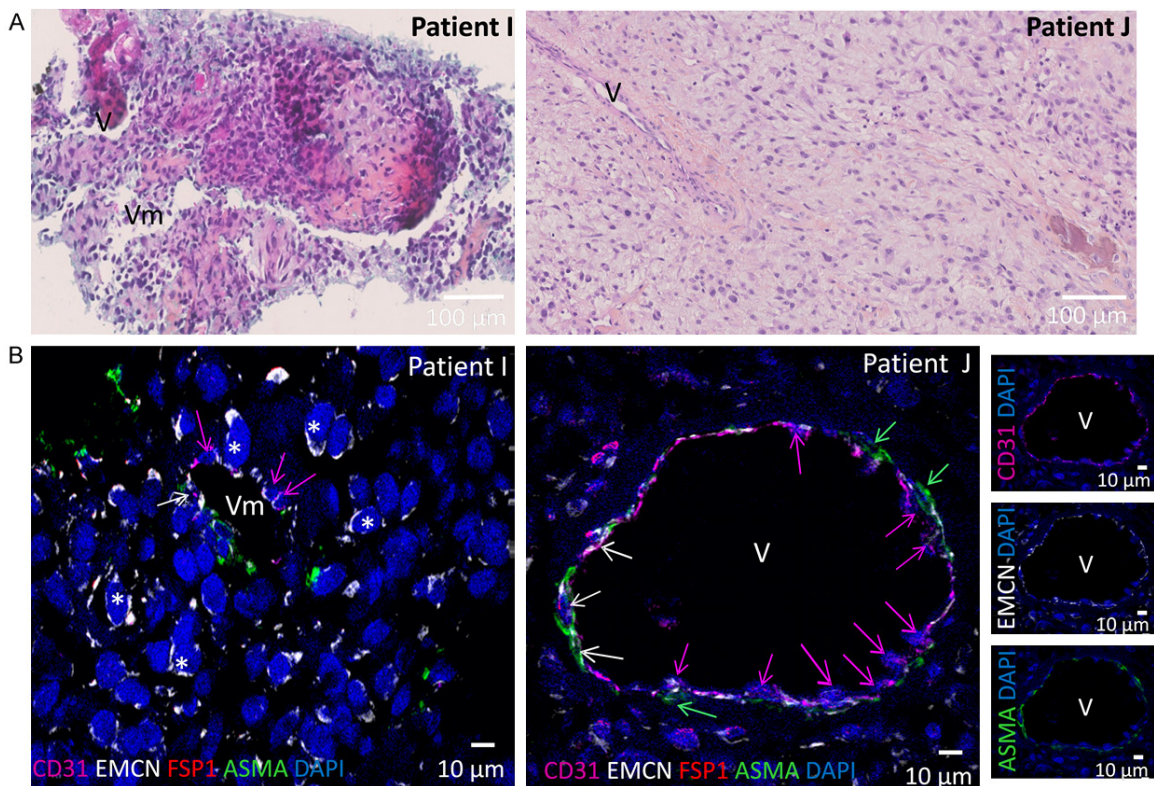
Figure 2. Representative microphotographies of multiplex immunofluorescent staining of vessels in osteosarcoma (OS) biopsies. A. Images of sample section after hematoxylin-eosin saffron staining showed osteoblastic and chondroblastic histological subtype of biopsies from patient I (left) and patient J (right). Scale Bars: 100 μm. B. Images of multiplexed immunofluorescent histochemistry. The color code for each specific fluorochrome was indicated in concordance with its marker CD31 (purple), EMCN (white), FSP1 (red), ASMA (green) and DNA labeling with DAPI (blue). Vascular mimicry was observed for vessel (Vm) with lumen lined by few tumor cells, while other vessel lumen (V) was lined by endothelial cells (ECs). Pink arrows showed nuclei of ECs expressing at least CD31 and possibly EMCN, whereas white arrows showed ECs expressing at least CD31 and the mesenchymal marker ASMA. Mesenchymal marker FSP1 was poorly detected for biopsies of patients I and J. Green arrows showed ASMA-positive cells identified as potential smooth muscle cells. Asterisks indicated some large nuclei of tumor cells expressing EMCN. Scale Bars: 10 μm.

able EndoMCs: in osteoblastic subtype OS from patient C and in osteoblastic and chondroblastic subtype OS from patients I and J, with respectively 42%, 10% and 17% of EndoMCs. In contrast, EndoMCs were not detected in 5 other patient's biopsies with various OS histological subtypes (osteoblastic for patients F and G, osteoblastic and chondroblastic for patients B and D, fibroblastic for patient H and telangiectatic for patient E) (**Table 2** and Supplementary Figure 1). While quantification revealed 10% of EndoMCs in biopsy of patient I, this patient's lung metastasis showed 32% of EndoMCs (**Table 2**). Similar percentages of ECs in mesenchymal transition were detected in biopsies of patient I (10%) and patient J (17%), both presented the same histological subtype

but identified as good (Patient I) and poor (Patient J) responder to NAPC.

Following treatment, only 3 resected tumor pieces revealed good histological integrity after HES staining and were used for immuno-detection by Opal ™ multiplexing. Remarkably, the resection pieces of patients A, B and H showed a very strong labeling for ASMA around vessels (**Figure 3** and Supplementary Figure 1), leading to the identification of ECs with mesenchymal markers in all resected samples with a range from 15% to 50% (**Table 2**). Notably for patient A, one vessel section was identified with 100% of ECs expressing CD31 and EMCN associated to ASMA (**Figure 3B**, left panels). For patient H, several vessels were observed
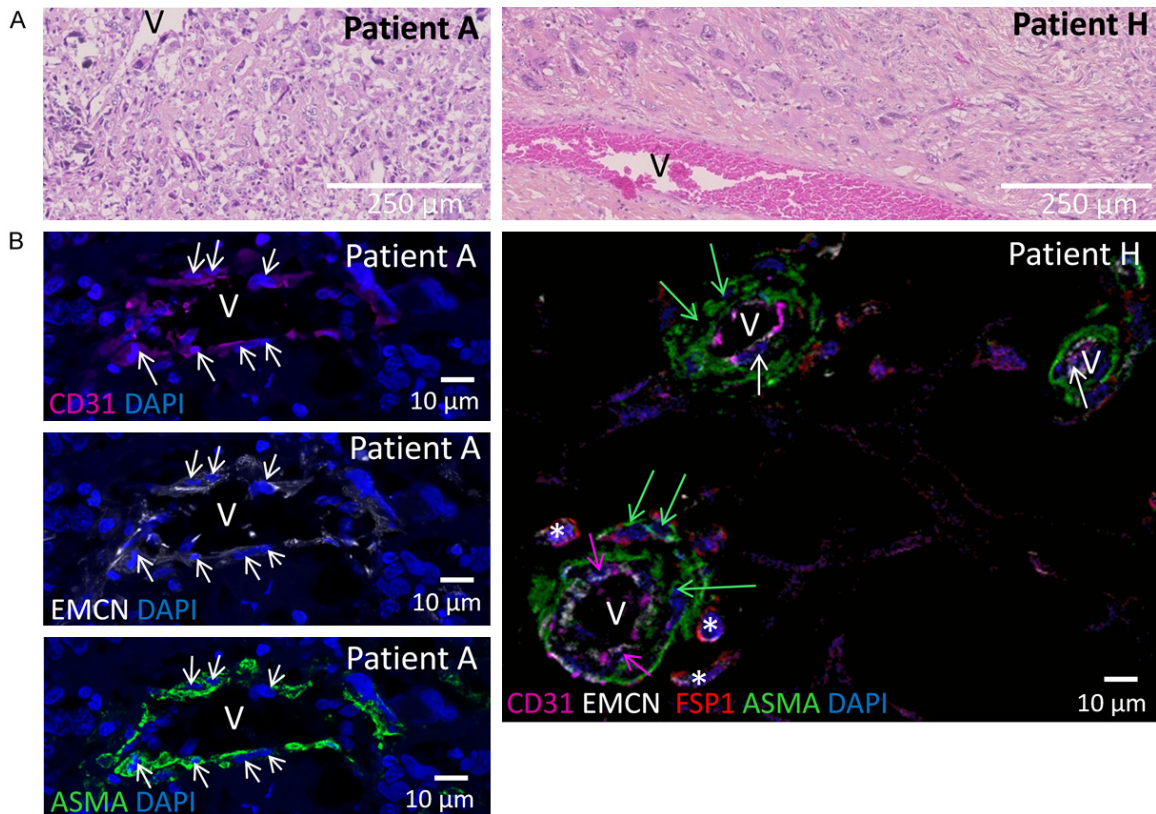
Figure 3. Representative microphotographies of multiplex immunofluorescent staining of vessels in osteosarcoma (OS) resection pieces following neo-adjuvant polychemotherapy (NAPC). A. Images of sample section after hematoxylin-eosin saffron staining showed osteoblastic and chondroblastic histological subtype of biopsies from patient A (left) and patient H (right). Scale Bars: 250 μm. B. Images of multiplexed immunofluorescent histochemistry. The color code for each specific fluorochrome was indicated in concordance with its marker. Vessels (V) were detected in the OS resection piece of patients A (left) and H (right). White arrows in patient A showed endothelial cells (ECs) co-expressing specific endothelial markers CD31 and EMCN and the mesenchymal marker ASMA. In sections from patient H, numerous arterioles were identified by a circular layer of ASMA-positive smooth muscle cells (nuclei are indicated by green arrows). Concerning the inner layer of vessels, pink arrows showed nuclei of ECs expressing CD31, associated with or without EMCN expression, whereas white arrows showed ECs co-expressing CD31 and mesenchymal marker ASMA. FSP1 mesenchymal marker was detected in association with some ASMA-expressing cells (green arrows) and with some tumor cells (asterisk), but not in association to endothelial marker CD31. Scale Bars: 10 μm.

with ASMA labeling around them, associated either to smooth muscle cells or to ECs (**Figure 3B**, right panel). Finally, only clearly distinguishable ECs expressing CD31 and co-stained with ASMA were counted, leading to 3 ECs into mesenchymal transition out of 6 ECs (**Table 2**). FSP1 mesenchymal marker was detected with some ASMA-expressing smooth muscle cells and some tumor cells (**Figure 3B**, right panel). The resection piece of patient B revealed 2 ECs associated with ASMA out of 13 ECs, highlighting a higher detection of ECs into mesenchymal transition in the resection sample compared to the biopsy of this patient, with 15% and no EndoMCs respectively (**Table 2**).

As we identified populations of ECs expressing mesenchymal markers in OS patients suggesting an EndoMT process in the tumor microenvironment, we then wanted to explore this process in depth in the context of OS by using *in vitro* approaches.

Secretome from OS cell lines induced an endothelial remodeling in HUVEC cells

Upon signals received from the tumor environment (either from cancer, stromal and/or immune cells), the endothelial vasculature may be remodeled, ultimately with ECs converted into fibroblasts-like cells through EndoMT.
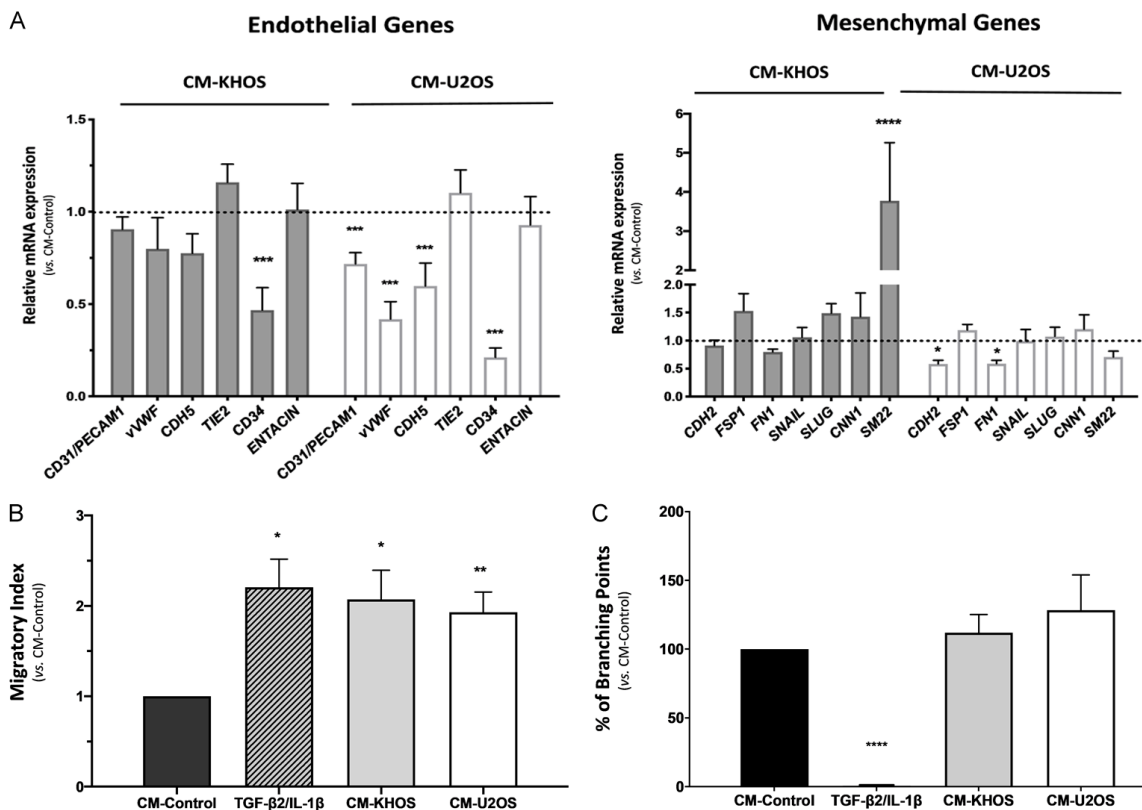
Figure 4. Effects of OS cell lines secretome on endothelial phenotype. Conditioned medium (CM) from OS cell lines KHOS or U2OS was incubated on HUVECs cells for 6 days. CM-control referred to no-cells unconditioned media. TGF-β2/IL-1β condition corresponded to CM-Control supplemented with 10 ng/mL of both cytokines. A. RT-qPCR analysis of endothelial and mesenchymal genes (N=8, n=3, *P<0.1, ***P<0.001, **** P<0.0001, compared to CM-Control condition). B. Quantification of Migration assay on HUVECs exposed 6 days to the different CMs (N=5, n=3, *P<0.1, **P<0.01, compared to CM-Control condition). C. Quantification of tubulogenesis assay on HUVECs exposed 6 days to CMs (N=5, ****P<0.0001, compared to CM-Control condition).

Therefore, we explored the secretome of OS cancer cells on endothelial cells HUVECs. We first validated that our model of HUVECs was able to fully transitioned to mesenchymal type and we showed that upon 6 days of treatment with known EndoMT inducers (TGF-β2 and IL-1β for 6 days, [18, 24]), HUVECs displayed the hallmarks of EndoMT: elongated morphology and stress fibers formation (Supplementary Figure 2A); decrease of expression of endothelial genes (Supplementary Figure 2B) and increase in mesenchymal genes and proteins (Supplementary Figure 2B and 2C), increased migratory properties (Supplementary Figure 2D) and loss of angiogenic capacities (Supplementary Figure 2E). HUVECs exposed to TGF-β2 and IL-1β for 6 days will be the positive control for fully achieved EndoMT.

Conditioned medium (CM) from the OS cell line KHOS (CM-KHOS) or U2OS (CM-U2OS) was then incubated on HUVECs for 6 days. CM-KHOS induced a decrease of endothelial *CD34* transcripts and an increase of mesenchymal *SM22* in HUVECs transcripts (**Figure 4A**). Impact of U2OS secretome was different, as HUVECs treated 6 days with CM-U2OS lowered almost all their endothelial markers (*CD31/ PECAM1, VWF, CDH5, CD34*) and this was not associated with an increased but rather with a decreased expression of mesenchymal marker matrix protein fibronectin 1 (*FN1*) and Neural Cadherin-2 (*CDH2*) transcripts (**Figure 4A**). HUVECs exposed to CM-KHOS or CM-U2OS migrated significantly more than those exposed to CM-control (**Figure 4B**), and to the same extend as HUVECs exposed to TGF-β2/IL-1β used here as EndoMT inducer (**Figure 4B**). Tubulogenesis assay revealed that HUVECs exposed to CM-KHOS or CM-U2OS formed an endothelial network with a number of branching points comparable to HUVECs exposed to
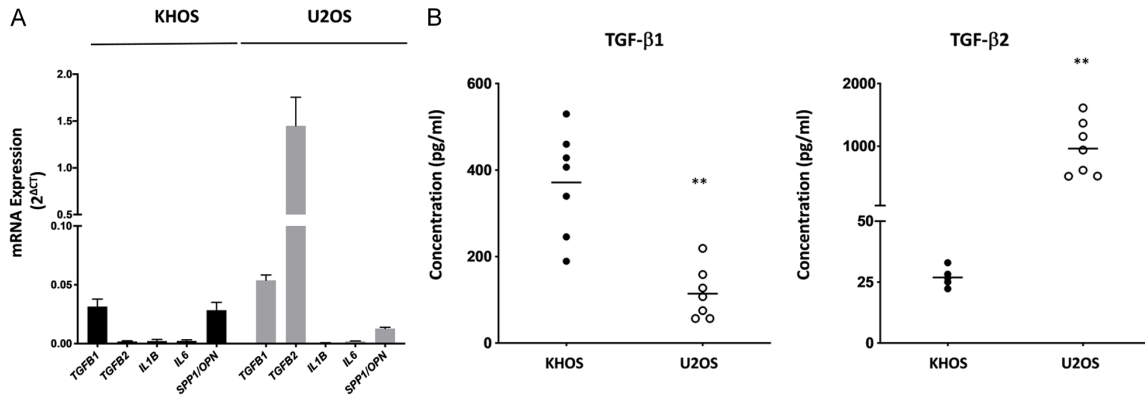
Figure 5. Detection of known pro-EndoMT factors expressed and/or secreted by OS cell lines KHOS and U2OS. A. mRNA expression of putative EndoMT-inducers factors in KHOS and U2OS osteosarcoma cell lines, analyzed by RT-qPCR analysis. B. Dosage of TGF-β1 and TGF-β2 secreted by OS cell lines by Bioplex technology (N=7, ***P<0.001, compared to KHOS).

CM-control (**Figure 4C**). On the opposite, ECs exposed to TGF-β2/IL-1β were unable to form tubules on Matrigel®.

In order to explore factors described to induce endothelial remodeling through EndoMT, that may be secreted by OS cell lines, we analyzed by RTqPCR the level of expression of several factors previously described as favoring EndoMT process in various tumor context, namely *TGFB1, TGFB2, IL1B, IL6, Osteopontin/ Secreted phosphoprotein-1 (OPN/SPP1)* [25]. Both KHOS and U2OS cell lines expressed *TGFB1* and *TGFB2* transcripts, with *TGFB1* at comparable levels and *TGFB2* more expressed in U2OS than in KHOS cell lines (**Figure 5A**). TGF-β1 and TGF-β2 were detected at the protein level in conditioned medium of both OS cell lines. The KHOS cell line expressed significantly more TGF-β1 than U2OS cells (371 ± 45 vs. 114 ± 22 pg /ml) but less TGF-β2 (29.6 ± 1.22 vs. 960 ± 164 pg/ml) (**Figure 5B**). *OPN/SPP1* transcripts were expressed in both cell lines but pro-inflammatory cytokines IL-1β and IL-6 were not detected in KHOS or U2OS cell lines (**Figure 5A**).

Secretome of normal or OS-derived mesenchymal stromal cells favored endothelial migration without promoting EndoMT

MSCs are described as a source of paracrine and autocrine factors involved in the modulation of the tumor ecosystem including tumor cells, bone cells, immune cells and endothelial cells especially in OS [26]. Factors described to induce endothelial remodeling through EndoMT such as TGF-βs [27] and several pro-inflammatory cytokines (IL-8, MCP-1, IL-6) have previously been identified as secreted by normal bone marrow MSCs or by tumor-associated MSCs [28-30]. As our group previously isolated and characterized mesenchymal stromal cells derived from human OS biopsy and termed OS patients-derived cells (OSDCs) [23], we next assessed whether the secretome of normal MSC (CM-MSC) or of OSDC (CM-OSDC) would influence the long-term remodeling of ECs.

Hallmarks of EndoMT were investigated in HUVECs exposed to CM-MSC or to CM-OSDC for 6 days. None conditioned media significantly affected endothelial and mesenchymal gene expression (**Figure 6A**). However, CM-MSC and CM-OSDC-treated HUVECs were more proned to migrate compared to cells treated with CM-control and they migrated to the same extend as cells exposed to TGF-β2/IL-1β (**Figure 6B**). Tubulogenesis assay showed that CM-MSC and CM-OSDC-treated HUVECs were organized into an endothelial network on Matrigel® with an identical number of branching points, as compared to CM-control-treated cells. This is in sharp contrast with ECs primed with TGF-β2/ IL-1β for 6 days, and thus engaged into the EndoMT process, that completely failed to form tubes (**Figure 6C**).

Discussion

The vascular microenvironment has a privileged place in the tumor ecosystem, as this
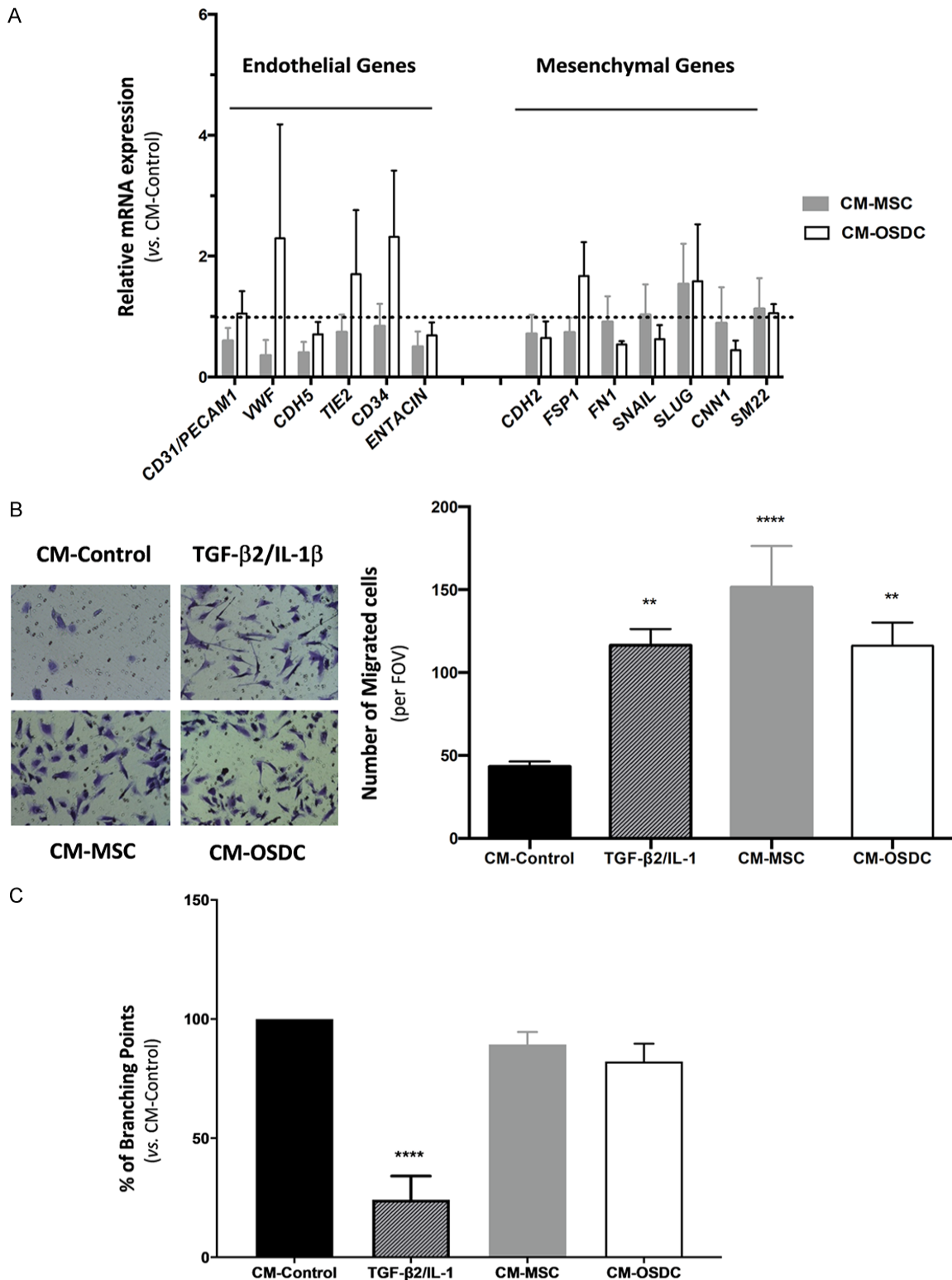
Figure 6. Effect of normal and OS-derived mesenchymal stromal cells conditioned medium on endothelial phenotype. Conditioned medium (CM) from normal (MSC) or OS-derived mesenchymal stromal cells (OSDC) was incubated on endothelial HUVEC cells for 6 days. CM-control referred to no-cells unconditioned medium. A. RT-qPCR analysis of endothelial and mesenchymal genes. (N=3, n=3, no significantly different, compared to CM-control condition). B. Migration of HUVECs exposed 6 days to TGF-β2/IL-1β, CM-MSC or CM-OSDC before migration assay. *(Right)* Images of migrated cells on Transwell after staining. *(Left)* Quantification of migrated cells expressed as mean of cells per field of view (FOV) (One representative experiment, n=19, **P<0.01; ****P<0.0001, compared to CM-control). C. Analysis of tubulogenesis assay on HUVECs exposed 6 days to CMs, expressed as % of branching points (N=4, ****P<0.0001, compared to CM-control).

compartment plays an essential role in tumor development and dissemination but also in resistance to therapies [31]. Despite that OS are tumors highly vascularized with vascular density identified as a hallmark of poor prognosis [32], the vascular microenvironment and its remodeling in OS remains insufficiently deciphered. This study highlights for the first time in the OS microenvironment the presence of CD31$^+$EMCN$^{+/-}$ endothelial cells expressing the mesenchymal marker ASMA in tissues samples from a cohort of 10 patients diagnosed with high-grade OS. These observations of endothelial-mesenchymal cells EndoMCs in patients may refer to intermediate transitional populations of the EndoMT process. Indeed, identifying the process of EndoMT in humans remains challenging, as it is inherently transitional and progressive, rendering difficult the detection of mesenchymal/fibroblastic cells originating from endothelium except if the transition is not fully achieved with endothelial markers still present. This may be the case for CD31$^+$EMCN$^{+/-}$ ASMA$^+$ cells we detected and for which we cannot predict the evolution by lack of experimental tracing. In contrast to EC-specific lineage tracing in mice models that rendered possible the exploration of EndoMT *in vivo* in cardiovascular diseases but also in cancer models [14, 16, 33], the only possibility to document EndoMT in human cancer samples remains the detection of those transitioning populations of cells co-expressing endothelial and mesenchymal markers. Several studies clearly described an EndoMT process in patients through detection of CD31$^+$/ASMA$^+$ cells in lung [14], colorectal [15], pancreas [34] cancers and in glioblastoma [35, 36] or CD31$^+$/FSP1$^+$ cells, as illustrated in melanoma [16] and glioblastoma [35]. With a similar approach, we identified CD31$^+$/ ASMA$^+$ endothelial-mesenchymal population in OS patient samples. FSP1, also known as S100A4, is considered a marker of activated fibroblasts in remodelling tissues, allowing the identification of carcinoma-associated fibroblasts (CAF), and a marker of EMT and EndoMT, as epithelial or endothelial cells have been detected with this unexpected mesenchymal marker. In our study, FSP1/S1004A was not detected associated to endothelial cells but was found in tumor cells of one tumor resection sample and in lung metastasis. The detection of FSP1 in sarcoma cells, by definition of mesenchymal origin, is less unexpected than in car-

cinoma cells. For osteosarcoma, one study described the expression of FSP1/S1004A in a clinical and pathological study including 120 human OS samples and showed that it was related to metastasis potency and poor response to chemotherapy [37].

Despite its small size, this new cohort is representative of the disease in terms of its histological heterogeneity (osteoblastic, chondroblastic, fibroblastic and telangiectatic), its primary location (5 distal femur, 2 proximal tibia and 2 humerus), its relatively poor response to NAPC (50% poor response) and severe metastatic progression in 50% of patients. The gender equality in this cohort may be related to the relatively young age of the cohort (15 years), the incidence of OS having previously been reported to be slightly higher and earlier in females for patients under 15 years of age [38]. Moreover, this new cohort allowed a multiplexing immunohistochemistry detection, as a soft decalcified solution has been used.

In this cohort, quantification of the EndoMCs in the biopsy samples was highly heterogenous, with patients with no EndoMCs (patients B, D, E, F, G), one patient with 42% of EndoMCs (patient C) and patients with a lower percentage of 10% and 17% EndoMCs (patients I and J). Analysis of patients' characteristics (age, histological subtype, location, metastasis at diagnosis, metastasis progression, response to neo-adjuvant chemotherapy) does not give any differential arguments to explain the heterogeneity of frequency of EndoMCs. Surprisingly, while EndoMT is described as a favoring factor for tumor dissemination in different cancers [17, 39, 40], no EndoMCs were detected in 3 biopsies (out of 4) from patients with metastasis progression, while 2 biopsies (out of 4) of patients with no metastatic progression displayed the highest percentages of EndoMCs (42% and 17%). These results suggest that presence of EndoMCs in biopsies at diagnosis may not be indicative of tumor dissemination in OS. Nevertheless, when comparing biopsy and metastasis samples (only available for patient I), the frequency of EndoMCs was 3-fold higher in the metastasis sample, suggesting that remodeling of endothelial cells with acquisition of mesenchymal features would be more supported in a metastatic microenvironment. Considering all samples included in this study, the

highest percentage of EndoMCs was overall found in resection pieces following polychemotherapy exposure, which is also consistent with several studies showing that therapies (chemo- or radiotherapy) favor endothelial remodeling up to an EndoMT [14, 41, 42].

In order to decipher more precisely endothelial remodeling through an EndoMT process in the OS context, at the cellular and molecular levels, we first defined HUVECs exposed to TGF-β2/IL-1β as an appropriate *in vitro* model recapitulating all the hallmarks of EndoMT. This model allowed to address the effects of secreted factors of two OS cell lines (KHOS and U2OS) in the induction of EndoMT in ECs. The secretome from KHOS cells induced a remodeling of ECs with mild mesenchymal features (decreased expression of *CD34* associated with increased *SM22*; increased motility but no loss of angiogenic capacities), suggesting an incomplete transitioning into a mesenchymal phenotype compatible with a partial EndoMT, as previously described [43] and recently confirmed by single cell sequencing approach in cardiac physiopathology [44]. Some authors considered the sprouting angiogenesis as a partial EndoMT, as early steps of sprouting recapitulate EndoMT characteristics [45, 46]. Similarly, by starting to express some mesenchymal markers and maintaining their angiogenic potential in Matrigel®, HUVECs exposed to CM-KHOS could be engaged towards an early step of angiogenesis. Secretome from U2OS cell line was not able to initiate an EndoMT process, as no increase of mesenchymal markers was induced. Differences between KHOS and U2OS cell lines have been described, mainly in their tumorigenicity and colony-forming ability [47] and in their *p53* status [48]; therefore, differences in the composition of their secretome, especially in potential EndoMT inducers, is more than probable. TGF-βs, known as canonical drivers of EndoMT [49], were detected in the serum of OS patients [50]. We confirmed the expression and secretion of TGF-β1 and TGF-β2 by both KHOS and U2OS cell lines, even though not to the same extend. Despite significant amounts of TGF-β1 and/or -β2 in the secretome of these cell lines, these cytokines were not sufficient on their own to lead to a complete EndoMT process. Additional factors, in particular inflammatory factors such as TNF-α, promoted EndoMT in HUVECs [51] and in microvas-

cular ECs [52]. Furthermore, combined with TGF-βs, pro-inflammatory cytokine IL-1β [18, 24] increased dramatically the EndoMT process. Therefore, in our experimental settings, as IL-1β was not detected in any secretome of OS cell lines, HUVECs may have lacked an inflammatory signal needed to complete the process of EndoMT.

In the OS tumor microenvironment, mesenchymal stromal cells (MSCs) are pillar actors [26]. MSCs sense but also modulate the environment and are involved in cellular communication toward OS tumor cells [53], immune cells [54] but also endothelial cells [55], mainly through secretion of soluble factors (cytokines and chemokines) and extracellular vesicles [56]. Therefore, we questioned the role played by soluble factors of normal MSCs and mesenchymal stromal cells derived from human OS biopsy (OSDC) on long-term exposure on HUVECs. None of the conditioned media (MSC or OSDC) was able to induce a complete EndoMT. Nevertheless, our results pointed the pro-migratory effect of both MSC or OSDC secretomes on ECs. Migration being an early step of angiogenesis, our results would favor a pro-angiogenic effect of MSC or OSDC secreted factors. This is in accordance with previous studies showing that MSCs produced several pro-angiogenic factors like VEGF [57]. Here again, necessary signals provided by other tumor microenvironment actors may be missing to complement MSCs secretome for efficient EndoMT induction. As previously illustrated [58], education of MSCs by direct contact with tumor cells could also be required for their full ability to promote EndoMT. In the microenvironment, immune cells could be a source of inflammatory factors and TGF-β. Anatomopathological analyses of high-grade OS have shown that T-lymphocytes and macrophages mainly compose the OS immune environment [59-62]. A mixture of TGF-β with different inflammatory cytokines (IL-1β, TNF-α, INF-β) seems relevant for reproducing *in vitro* certain interactions between tumor cells and non-tumor cells. Therefore, many combinations of cell communication may be envisaged to mimic all the intra- and inter- heterogeneity of high-grade OS, as illustrated by our histological study and 3D-model cultures could be helpful to understand the endothelial plasticity in OS context.

In conclusion, this study demonstrated for the first time that the endothelial compartment of human OS microenvironment is able to acquire mesenchymal features, suggesting a commitment toward an EndoMT process. This work needs now to be extended to a larger cohort of OS samples, in order to strengthen these first observations that EndoMC pool of cells could be related to the progression and resistance of the tumor. Furthermore, identification of tumor factors and cells able to promote some remodeling of endothelial cells in our model suggest a role for some education of the tumor vascular microenvironment of OS by tumor cells that deserved further investigation.

Acknowledgements

Disclosure of conflict of interest

None.

Address correspondence to: Valérie Trichet and Isabelle Corre, Nantes Université, Inserm UMR 1238, F-44000 Nantes, France. E-mail: valerie.trichet@univ-nantes.fr (VT); isabelle.corre@univ-nantes.fr (IC)

References

[1] Kansara M, Teng MW, Smyth MJ and Thomas DM. Translational biology of osteosarcoma. Nat Rev Cancer 2014; 14: 722-735.

[2] Gaebler M, Silvestri A, Haybaeck J, Reichardt P, Lowery CD, Stancato LF, Zybarth G and Regenbrecht CRA. Three-dimensional patient-derived in vitro sarcoma models: promising tools for improving clinical tumor management. Front Oncol 2017; 7: 203.

[3] Matsushita Y, Liu J, Chu AKY, Tsutsumi-Arai C, Nagata M, Arai Y, Ono W, Yamamoto K, Saunders TL, Welch JD and Ono N. Bone marrow endosteal stem cells dictate active osteogenesis and aggressive tumorigenesis. Nat Commun 2023; 14: 2383.

[4] Mutsaers AJ and Walkley CR. Cells of origin in osteosarcoma: mesenchymal stem cells or osteoblast committed cells? Bone 2014; 62: 56-63.

[5] Allison DC, Carney SC, Ahlmann ER, Hendifar A, Chawla S, Fedenko A, Angeles C and Menendez LR. A meta-analysis of osteosarcoma outcomes in the modern medical era. Sarcoma 2012; 2012: 704872.

[6] Gaspar N, Di Giannatale A, Geoerger B, Redini F, Corradini N, Enz-Werle N, Tirode F, Marec-Berard P, Gentet JC, Laurence V, Piperno-Neumann S, Oberlin O and Brugieres L. Bone sarcomas: from biology to targeted therapies. Sarcoma 2012; 2012: 301975.

[7] Gianferante DM, Mirabello L and Savage SA. Germline and somatic genetics of osteosarcoma - connecting aetiology, biology and therapy. Nat Rev Endocrinol 2017; 13: 480-491.

[8] Paget S. The distribution of secondary growths in cancer of the breast. 1889. Cancer Metastasis Rev 1989; 8: 98-101.

[9] Hanahan D and Weinberg RA. Hallmarks of cancer: the next generation. Cell 2011; 144: 646-674.

[10] Charity RM, Foukas AF, Deshmukh NS and Grimer RJ. Vascular endothelial growth factor expression in osteosarcoma. Clin Orthop Relat Res 2006; 448: 193-198.

[11] Chen D, Zhang YJ, Zhu KW and Wang WC. A systematic review of vascular endothelial growth factor expression as a biomarker of prognosis in patients with osteosarcoma. Tumour Biol 2013; 34: 1895-1899.

[12] Liebner S, Cattelino A, Gallini R, Rudini N, Iurlaro M, Piccolo S and Dejana E. Beta-catenin is required for endothelial-mesenchymal transformation during heart cushion development in the mouse. J Cell Biol 2004; 166: 359-367.

[13] Deng Y, Guo Y, Liu P, Zeng R, Ning Y, Pei G, Li Y, Chen M, Guo S, Li X, Han M and Xu G. Blocking protein phosphatase 2A signaling prevents endothelial-to-mesenchymal transition and renal fibrosis: a peptide-based drug therapy. Sci Rep 2016; 6: 19821.

[14] Choi SH, Kim AR, Nam JK, Kim JM, Kim JY, Seo HR, Lee HJ, Cho J and Lee YJ. Tumour-vasculature development via endothelial-to-mesenchymal transition after radiotherapy controls CD44v6+ cancer cell and macrophage polarization. Nat Commun 2018; 9: 5108.

[15] Fan CS, Chen WS, Chen LL, Chen CC, Hsu YT, Chua KV, Wang HD and Huang TS. Osteopontin-integrin engagement induces HIF-1α-TCF12-mediated endothelial-mesenchymal transition to exacerbate colorectal cancer. Oncotarget 2017; 9: 4998-5015.

[16] Zeisberg EM, Potenta S, Xie L, Zeisberg M and Kalluri R. Discovery of endothelial to mesenchymal transition as a source for carcinoma-associated fibroblasts. Cancer Res 2007; 67: 10123-10128.

[17] Gasparics Á, Rosivall L, Krizbai IA and Sebe A. When the endothelium scores an own goal: endothelial cells actively augment metastatic extravasation through endothelial-mesenchymal transition. Am J Physiol Heart Circ Physiol 2016; 310: H1055-1063.

[18] Nie L, Lyros O, Medda R, Jovanovic N, Schmidt JL, Otterson MF, Johnson CP, Behmaram B, Shaker R and Rafiee P. Endothelial-mesenchymal transition in normal human esophageal endothelial cells cocultured with esophageal adenocarcinoma cells: role of IL-1β and TGF-β2. Am J Physiol Cell Physiol 2014; 307: C859-C877.

[19] Zeisberg EM, Tarnavski O, Zeisberg M, Dorfman AL, McMullen JR, Gustafsson E, Chandraker A, Yuan X, Pu WT, Roberts AB, Neilson EG, Sayegh MH, Izumo S and Kalluri R. Endothelial-to-mesenchymal transition contributes to cardiac fibrosis. Nat Med 2007; 13: 952-961.

[20] Wei WF, Zhou HL, Chen PY, Huang XL, Huang L, Liang LJ, Guo CH, Zhou CF, Yu L, Fan LS and Wang W. Cancer-associated fibroblast-derived PAI-1 promotes lymphatic metastasis via the induction of EndoMT in lymphatic endothelial cells. J Exp Clin Cancer Res 2023; 42: 160.

[21] Kusumbe AP, Ramasamy SK and Adams RH. Coupling of angiogenesis and osteogenesis by a specific vessel subtype in bone. Nature 2014; 507: 323-328.

[22] Miquelestorena-Standley E, Jourdan ML, Collin C, Bouvier C, Larousserie F, Aubert S, Gomez-Brouchet A, Guinebretière JM, Tallegas M, Brulin B, Le Nail LR, Tallet A, Le Loarer F, Massiere J, Galant C and de Pinieux G. Effect of decalcification protocols on immunohistochemistry and molecular analyses of bone samples. Mod Pathol 2020; 33: 1505-1517.

[23] Le Nail LR, Brennan M, Rosset P, Deschaseaux F, Piloquet P, Pichon O, Le Caignec C, Crenn V, Layrolle P, Hérault O, De Pinieux G and Trichet V. Comparison of tumor- and bone marrow-derived mesenchymal stromal/stem cells from patients with high-grade osteosarcoma. Int J Mol Sci 2018; 19: 707.

[24] Maleszewska M, Moonen JR, Huijkman N, van de Sluis B, Krenning G and Harmsen MC. IL-1β and TGFβ2 synergistically induce endothelial to mesenchymal transition in an NFκB-dependent manner. Immunobiology 2013; 218: 443-54.

[25] Clere N, Renault S and Corre I. Endothelial-to-mesenchymal transition in cancer. Front Cell Dev Biol 2020; 8: 747.

[26] Corre I, Verrecchia F, Crenn V, Redini F and Trichet V. The osteosarcoma microenvironment: a complex but targetable ecosystem. Cells 2020; 9: 976.

[27] Di Nicola M, Carlo-Stella C, Magni M, Milanesi M, Longoni PD, Matteucci P, Grisanti S and Gianni AM. Human bone marrow stromal cells suppress T-lymphocyte proliferation induced by cellular or nonspecific mitogenic stimuli. Blood 2002; 99: 3838-3843.

[28] Petrenko Y, Vackova I, Kekulova K, Chudickova M, Koci Z, Turnovcova K, Kupcova Skalnikova H, Vodicka P and Kubinova S. A comparative analysis of multipotent mesenchymal stromal cells derived from different sources, with a focus on neuroregenerative potential. Sci Rep 2020; 10: 4290.

[29] Cortini M, Massa A, Avnet S, Bonuccelli G and Baldini N. Tumor-activated mesenchymal stromal cells promote osteosarcoma stemness and migratory potential via IL-6 secretion. PLoS One 2016; 11: e0166500.

[30] Corre J, Labat E, Espagnolle N, Hébraud B, Avet-Loiseau H, Roussel M, Huynh A, Gadelorge M, Cordelier P, Klein B, Moreau P, Facon T, Fournié JJ, Attal M and Bourin P. Bioactivity and prognostic significance of growth differentiation factor GDF15 secreted by bone marrow mesenchymal stem cells in multiple myeloma. Cancer Res 2012; 72: 1395-1406.

[31] Quail DF and Joyce JA. Microenvironmental regulation of tumor progression and metastasis. Nat Med 2013; 19: 1423-1437.

[32] Dumars C, Ngyuen JM, Gaultier A, Lanel R, Corradini N, Gouin F, Heymann D and Heymann MF. Dysregulation of macrophage polarization is associated with the metastatic process in osteosarcoma. Oncotarget 2016; 7: 78343-78354.

[33] Li Y, Lui KO and Zhou B. Reassessing endothelial-to-mesenchymal transition in cardiovascular diseases. Nat Rev Cardiol 2018; 15: 445-456.

[34] Fan CS, Chen LL, Hsu TA, Chen CC, Chua KV, Li CP and Huang TS. Endothelial-mesenchymal transition harnesses HSP90α-secreting M2-macrophages to exacerbate pancreatic ductal adenocarcinoma. J Hematol Oncol 2019; 12: 138.

[35] Huang M, Liu T, Ma P, Mitteer RA Jr, Zhang Z, Kim HJ, Yeo E, Zhang D, Cai P, Li C, Zhang L, Zhao B, Roccograndi L, O'Rourke DM, Dahmane N, Gong Y, Koumenis C and Fan Y. c-Met-mediated endothelial plasticity drives aberrant vascularization and chemoresistance in glioblastoma. J Clin Invest 2016; 126: 1801-1814.

[36] Huang M, Zhang D, Wu JY, Xing K, Yeo E, Li C, Zhang L, Holland E, Yao L, Qin L, Binder ZA, O'Rourke DM, Brem S, Koumenis C, Gong Y and Fan Y. Wnt-mediated endothelial transformation into mesenchymal stem cell-like cells induces chemoresistance in glioblastoma. Sci Transl Med 2020; 12: eaay7522.

[37] Cao CM, Yang FX, Wang PL, Yang QX and Sun XR. Clinicopathologic significance of S100A4 expression in osteosarcoma. Eur Rev Med Pharmacol Sci 2014; 18: 833-839.

[38] Mirabello L, Troisi RJ and Savage SA. Osteosarcoma incidence and survival rates from 1973 to 2004: data from the Surveillance, Epidemiology, and End Results Program. Cancer 2009; 115: 1531-1543.

[39] Anderberg C, Cunha SI, Zhai Z, Cortez E, Pardali E, Johnson JR, Franco M, Páez-Ribes M, Cordiner R, Fuxe J, Johansson BR, Goumans MJ, Casanovas O, ten Dijke P, Arthur HM and Pietras K. Deficiency for endoglin in tumor vasculature weakens the endothelial barrier to metastatic dissemination. J Exp Med 2013; 210: 563-579.

[40] Tanaka M, Koyama T, Sakurai T, Kamiyoshi A, Ichikawa-Shindo Y, Kawate H, Liu T, Xian X, Imai A, Zhai L, Hirabayashi K, Owa S, Yamauchi A, Igarashi K, Taniguchi S and Shindo T. The endothelial adrenomedullin-RAMP2 system regulates vascular integrity and suppresses tumour metastasis. Cardiovasc Res 2016; 111: 398-409.

[41] Kim SH, Song Y and Seo HR. GSK-3β regulates the endothelial-to-mesenchymal transition via reciprocal crosstalk between NSCLC cells and HUVECs in multicellular tumor spheroid models. J Exp Clin Cancer Res 2019; 38: 46.

[42] Liu T, Ma W, Xu H, Huang M, Zhang D, He Z, Zhang L, Brem S, O'Rourke DM, Gong Y, Mou Y, Zhang Z and Fan Y. PDGF-mediated mesenchymal transformation renders endothelial resistance to anti-VEGF treatment in glioblastoma. Nat Commun 2018; 9: 3439.

[43] Dejana E, Hirschi KK and Simons M. The molecular basis of endothelial cell plasticity. Nat Commun 2017; 8: 14361.

[44] Tombor LS, John D, Glaser SF, Luxán G, Forte E, Furtado M, Rosenthal N, Baumgarten N, Schulz MH, Wittig J, Rogg EM, Manavski Y, Fischer A, Muhly-Reinholz M, Klee K, Looso M, Selignow C, Acker T, Bibli SI, Fleming I, Patrick R, Harvey RP, Abplanalp WT and Dimmeler S. Single cell sequencing reveals endothelial plasticity with transient mesenchymal activation after myocardial infarction. Nat Commun 2021; 12: 681.

[45] Welch-Reardon KM, Wu N and Hughes CC. A role for partial endothelial-mesenchymal transitions in angiogenesis? Arterioscler Thromb Vasc Biol 2015; 35: 303-308.

[46] Fang JS, Hultgren NW and Hughes CCW. Regulation of partial and reversible endothelial-to-mesenchymal transition in angiogenesis. Front Cell Dev Biol 2021; 9: 702021.

[47] Lauvrak SU, Munthe E, Kresse SH, Stratford EW, Namløs HM, Meza-Zepeda LA and Myklebost O. Functional characterisation of osteosarcoma cell lines and identification of mRNAs and miRNAs associated with aggressive cancer phenotypes. Br J Cancer 2013; 109: 2228-2236.

[48] Ottaviano L, Schaefer KL, Gajewski M, Huckenbeck W, Baldus S, Rogel U, Mackintosh C, de Alava E, Myklebost O, Kresse SH, Meza-Zepeda LA, Serra M, Cleton-Jansen AM, Hogendoorn PC, Buerger H, Aigner T, Gabbert HE and Poremba C. Molecular characterization of commonly used cell lines for bone tumor research: a trans-European EuroBoNet effort. Genes Chromosomes Cancer 2010; 49: 40-51.

[49] Ma J, Sanchez-Duffhues G, Goumans MJ and Ten Dijke P. TGF-β-induced endothelial to mesenchymal transition in disease and tissue engineering. Front Cell Dev Biol 2020; 8: 260.

[50] Lamora A, Talbot J, Bougras G, Amiaud J, Leduc M, Chesneau J, Taurelle J, Stresing V, Le Deley MC, Heymann MF, Heymann D, Redini F and Verrecchia F. Overexpression of Smad7 blocks primary tumor growth and lung metastasis development in osteosarcoma. Clin Cancer Res 2014; 20: 5097-5112.

[51] Ciavarella C, Motta I, Vasuri F, Fittipaldi S, Valente S, Pollutri D, Ricci F, Gargiulo M and Pasquinelli G. Involvement of miR-30a-5p and miR-30d in endothelial to mesenchymal transition and early osteogenic commitment under inflammatory stress in HUVEC. Biomolecules 2021; 11: 226.

[52] Adjuto-Saccone M, Soubeyran P, Garcia J, Audebert S, Camoin L, Rubis M, Roques J, Binétruy B, Iovanna JL and Tournaire R. TNF-α induces endothelial-mesenchymal transition promoting stromal development of pancreatic adenocarcinoma. Cell Death Dis 2021; 12: 649.

[53] Lazennec G and Lam PY. Recent discoveries concerning the tumor - mesenchymal stem cell interactions. Biochim Biophys Acta 2016; 1866: 290-299.

[54] Humbert P, Brennan MÁ, De Lima J, Brion R, Adrait A, Charrier C, Brulin B, Trichet V, Couté Y, Blanchard F and Layrolle P. Apoptotic mesenchymal stromal cells support osteoclastogenesis while inhibiting multinucleated giant cells formation in vitro. Sci Rep 2021; 11: 12144.

[55] Bronckaers A, Hilkens P, Martens W, Gervois P, Ratajczak J, Struys T and Lambrichts I. Mesenchymal stem/stromal cells as a pharmacological and therapeutic approach to accelerate angiogenesis. Pharmacol Ther 2014; 143: 181-196.

[56] Ruiz M, Toupet K, Maumus M, Rozier P, Jorgensen C and Noël D. TGFBI secreted by mesenchymal stromal cells ameliorates osteo-

arthritis and is detected in extracellular vesicles. Biomaterials 2020; 226: 119544.

[57] Boomsma RA and Geenen DL. Mesenchymal stem cells secrete multiple cytokines that promote angiogenesis and have contrasting effects on chemotaxis and apoptosis. PLoS One 2012; 7: e35685.

[58] Pietrovito L, Leo A, Gori V, Lulli M, Parri M, Becherucci V, Piccini L, Bambi F, Taddei ML and Chiarugi P. Bone marrow-derived mesenchymal stem cells promote invasiveness and transendothelial migration of osteosarcoma cells via a mesenchymal to amoeboid transition. Mol Oncol 2018; 12: 659-676.

[59] Buddingh EP, Kuijjer ML, Duim RA, Bürger H, Agelopoulos K, Myklebost O, Serra M, Mertens F, Hogendoorn PC, Lankester AC and Cleton-Jansen AM. Tumor-infiltrating macrophages are associated with metastasis suppression in high-grade osteosarcoma: a rationale for treatment with macrophage activating agents. Clin Cancer Res 2011; 17: 2110-2119.

[60] Han Q, Shi H and Liu F. CD163(+) M2-type tumor-associated macrophage support the suppression of tumor-infiltrating T cells in osteosarcoma. Int Immunopharmacol 2016; 34: 101-106.

[61] Ratti C, Botti L, Cancila V, Galvan S, Torselli I, Garofalo C, Manara MC, Bongiovanni L, Valenti CF, Burocchi A, Parenza M, Cappetti B, Sangaletti S, Tripodo C, Scotlandi K, Colombo MP and Chiodoni C. Trabectedin overrides osteosarcoma differentiative block and reprograms the tumor immune environment enabling effective combination with immune checkpoint inhibitors. Clin Cancer Res 2017; 23: 5149-5161.

[62] Gomez-Brouchet A, Illac C, Gilhodes J, Bouvier C, Aubert S, Guinebretiere JM, Marie B, Larousserie F, Entz-Werlé N, de Pinieux G, Filleron T, Minard V, Minville V, Mascard E, Gouin F, Jimenez M, Ledeley MC, Piperno-Neumann S, Brugieres L and Rédini F. CD163-positive tumor-associated macrophages and CD8-positive cytotoxic lymphocytes are powerful diagnostic markers for the therapeutic stratification of osteosarcoma patients: an immunohistochemical analysis of the biopsies fromthe French OS2006 phase 3 trial. Oncoimmunology 2017; 6: e1331193.

Supplementary Table 1. Sequences of Primers used for RTqPCR

Target	Forward	Reverse
CD31/PECAM	AGACGTGCAGTACACGGAAG	TTTCCACGGCATCAGGGAC
VWF	TGCAGGGGAAGATGATTCCTG	GTCACTTCCGAAAAGGCTGC
CDH5	GAAGCCTCTGATTGGCACAGTG	TTTTGTGACTCGGAAGAACTGGC
TIE2	GGTCAAGCAACCCAGCCTTTTC	CAGGTCATTCCAGCAGAGCCAA
CD34	TCCTAAGTGACATCAAGGCAGAAA	CCCTCTCCCCTGTCCTTCTTA
Entacin	AACGTGTGTGGCTGTCGT	GCTGGGGTATGTCGCAGTTA
CDH2	AGGCTTCTGGTGAAATCGCA	GCAGTTGCTAAACTTCACATTGAG
FSP1	GCTTCTTGGGGAAAAGGACAGA	GAAGTCCACCTCGTTGTCCC
FN1	AACATGGTTTTAGGCGGACC	TTCTTGTCCTACATTCGGCG
SNAIL1	AATCCAGAGTTTACCTTCCAGCA	TCCCAGATGAGCATTGGCAG
SLUG1	TGGTTGCTTCAAGGACACAT	GCAAATGCTCTGTTGCAGTG
CNN1	TTTGAGGCCAACGACCTGTT	TCCTTTCGTCTTCGCCATGC
SM22	CAGTGTGGCCCTGATGTG	CACCAGCTTGCTCAGAATCA
HPRT	TGACCTTGATTTATTTTGCATACC	CGAGCAAGACGTTCAGTCCT
B2M	TTCTGGCCTGGAGGCTATC	TCAGGAAATTTGACTTTCCATTC
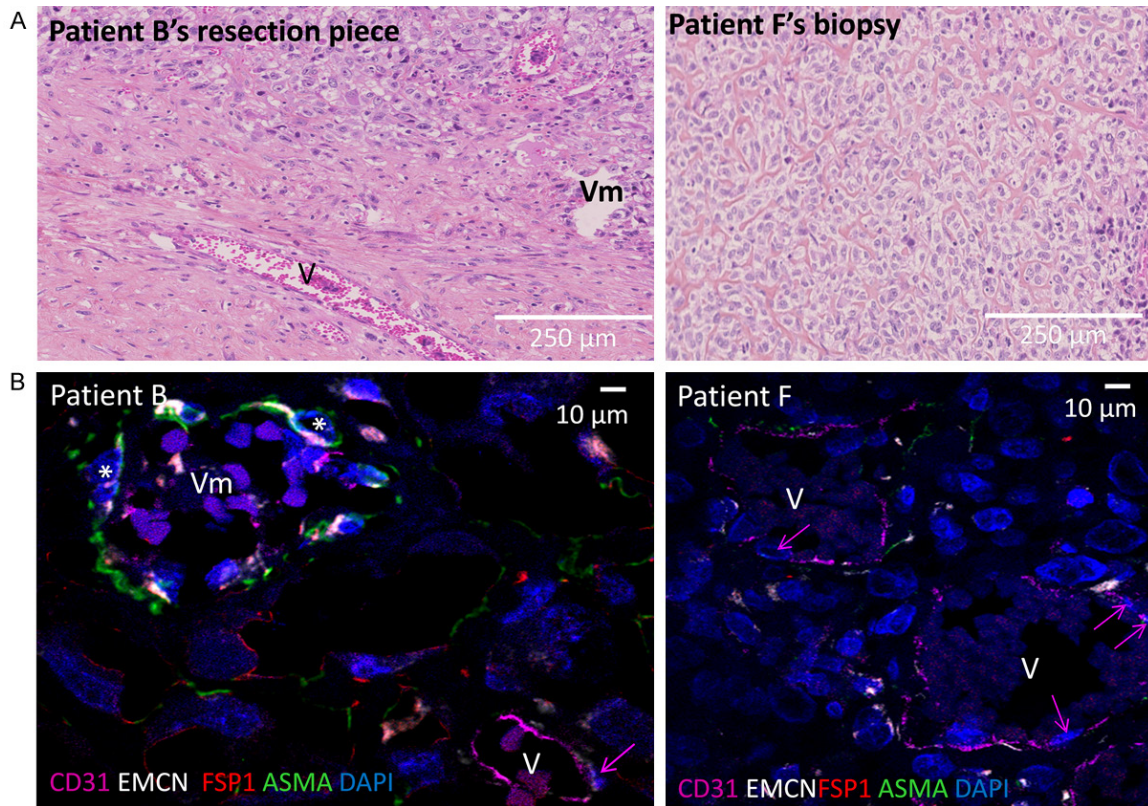
Supplementary Figure 1. Representative microphotographies of vessels in osteosarcoma (OS) samples. A. Images of sample sections after hematoxylin-eosin saffron staining for resection piece of patient B (left panel) and biopsy of patient F (right panel). Vessel lumen lined by tumor cells was indicated Vm in contrast to other vessel lumen (V) lined only by endothelial cells (ECs). Patient B's sample showed a weak necrosis (picnotic nuclei) following neo-adjuvant polychemotherapy. Patient F's biopsy showed an abundant osteoid matrix. Scale Bar: 250 µm. B. Images of multiplexed immunofluorescent histochemistry for patients B and F's samples. The color code for each specific fluorochrome was indicated in concordance with its marker. Pink arrow indicated nucleus of an EC expressing CD31. Lumen of the vessel noted Vm was lined partially by tumor cells characterized by a large nucleus (white asterisk), positively labeled for mesenchymal markers (ASMA and FSP1) but poorly associated to CD31 marker. Scale Bars: 10 µm.
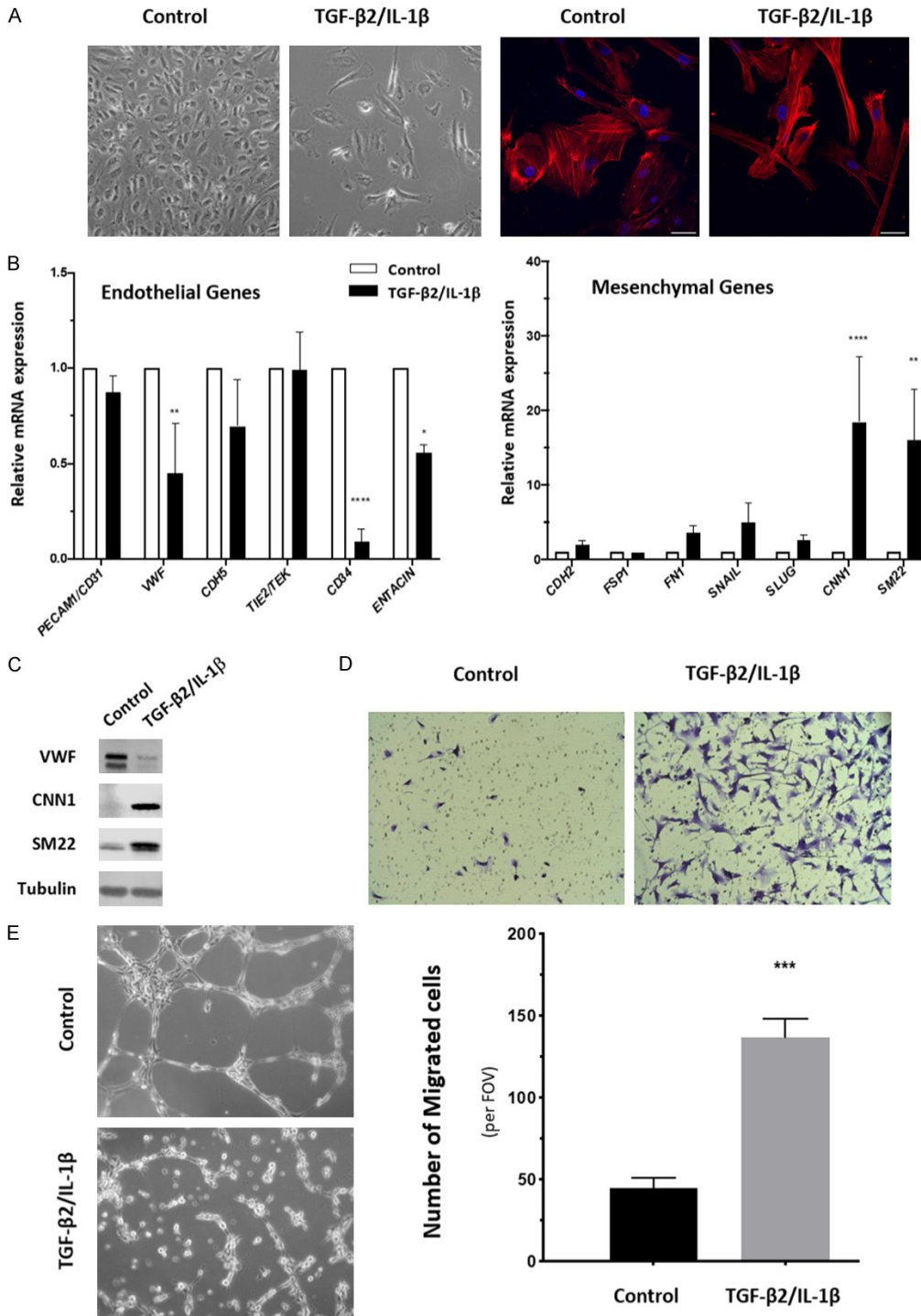
Supplementary Figure 2. Hallmarks of EndoMT in HUVECs exposed to TGF-β2 and IL-1β. HUVECs were treated or not (Control) with 10 ng/ml of TGF-β2 and IL-1β for 6 days. A. *(Left)* Brightfield microscopy images of HUVECs, Magnification ×100 *(Right)* Fluorescence microscopy analysis of actin cytoskeleton stained with Phalloidin-Alexa 568 (red). Nuclei were stained with Dapi (blue). Scale Bar: 40 μm. B. RT-qPCR analysis of endothelial and mesenchymal genes. Expression levels were normalized to two housekeeping genes (N=4 (biological replicates), n=3 (technical replicates), **P<0.01, ****P<0.0001, compared to Control condition). C. Expression of endothelial (VWF) and mesenchymal (CNN1, SM22) proteins revealed by Western blot. Tubulin was used as loading control. Blot representative of 3 experiments. D. Images of TGF-β2/IL-1β-treated HUVECs that had migrated on Transwell Boyden chamber upon serum gradient, and then fixed and stained. Quantification of migrated cells was expressed as mean of cells per field of view (FOV) (N=3 (biological replicates), n=17 (number of cells/field) ***P<0.001, compared to Control condition). E. Brightfield microscopy images of TGF-β2/IL-1β-treated HUVECs in tubulogenesis assay on Matrigel® for 6 hours. Magnification ×100.